J Mater Sci: Mater Electron
DOI 10.1007/s10854-016-4697-9

Microwave dielectric properties of low temperature sintering $Ca_5Mn_4(VO_4)_6$ ceramics

Guo-guang Yao[1] · Cui-Jin Pei[1] · Peng Liu[2] · Jian-ping Zhou[2] · Huai-wu Zhang[3]

Received: 20 December 2015 / Accepted: 14 March 2016

Abstract Low temperature sinterable $Ca_5Mn_4(VO_4)_6$ ceramics were fabricated by the conventional solid-state reaction route and their microwave dielectric properties were investigated for the first time. The formation of $Ca_5Mn_4(VO_4)_6$ main phase was confirmed by XRD diffraction pattern. The correlations between sintering temperature, packing fraction, and microwave dielectric properties in $Ca_5Mn_4(VO_4)_6$ ceramics were also studied. The $Ca_5Mn_4(VO_4)_6$ ceramics sintered at 875 °C for 5 h possessed good microwave dielectric properties: $\varepsilon_r = 11.2$, $Q \times f = 33,800$ GHz (at 10.5 GHz) and $\tau_f = -70$ ppm/°C. The material was found to react seriously with Ag when sintered at 875 °C, forming $(AgCa_2)Mn_2(VO_4)_3$ phase.

1 Introduction

The continuous improvements in wireless telecommunication systems demand development of new materials and methods for circuit miniaturization. Especially, advanced substrate materials with a low dielectric constant (ε_r), a high quality factor ($Q \times f$), and a near-zero temperature coefficient of resonant frequency (τ_f) are receiving increased interest [1, 2]. In addition, the low temperature cofired ceramic (LTCC) technology has been widely investigated due to significant benefits over other established packaging technologies for low-cost and miniaturization in the microwave devices [3, 4]. To meet the requirement of LTCC technology, the materials must have lower sintering temperature than the melting point of Ag electrode (960 °C). Therefore, the advanced substrate materials of LTCC systems should have a lower sintering temperature and possess excellent performance. At present, the major challenge in LTCC technology is the reducing the sintering temperature (below 900 °C) of the ceramic without affecting its dielectric performance.

The current trend is to develop genuine low firing ceramics and the most recent investigations have explored the applicability of garnet structure compounds containing vanadium element, which show some interesting physical properties such as dielectric and luminescence [5–10]. In our previous work, the $Ca_5A_4(VO_4)_6$ (A = Mg, Zn, Co) ceramics sintered at below 900 °C exhibited good microwave dielectric properties [11, 12]. Mn^{2+} exhibits an equal electro valence and similar ionic radius to that of A^{2+} in $Ca_5A_4(VO_4)_6$ (A = Mg, Zn, Co) system, however, no detail structural analysis and microwave dielectric properties of $Ca_5Mn_4(VO_4)_6$ have been reported. In this study, $Ca_5Mn_4(VO_4)_6$ ceramics were prepared by the traditional solid-state reaction route. The sintering behavior, crystal structure and microwave dielectric properties of $Ca_5Mn_4(VO_4)_6$ ceramics were studied for the first time. The chemical compatibility of $Ca_5Mn_4(VO_4)_6$ with silver electrode was also investigated.

✉ Guo-guang Yao
yaoguoguang@xupt.edu.cn

✉ Peng Liu
liupeng@snnu.edu.cn

[1] School of Science, Xi'an University of Posts and Telecommunications, Xi'an 710121, China

[2] College of Physics and Information Technology, Shaanxi Normal University, Xi'an 710062, China

[3] The Key Laboratory of Electronic Thin Film and Integrated Device, University of Electronic Science and Technology of China, Chengdu 610054, China

Published online: 25 March 2016

2 Experimental procedure

Samples of the $Ca_5Mn_4(VO_4)_6$ ceramics were synthesized by a conventional solid-state method using high-purity oxide powders (>99 %): $MnCO_3$, $CaCO_3$ and V_2O_5. The pre-dried raw materials were mixed according to the desired stoichiometry of the $Ca_5Mn_4(VO_4)_6$ ceramics. The powders were ground for 8 h in a nylon jar with agate balls and ethanol as media. The $Ca_5Mn_4(VO_4)_6$ powders were calcined at 800 °C for 3 h. The calcined powders were reground for 8 h, dried, mixed with 5 wt% PVA as a binder, and granulated. The granulated powders were uniaxially pressed into pellets with 10 mm in diameter and 4–5 mm in height under the pressure of 200 MPa. These pellets were sintered from 825 to 900 °C for 5 h in air with a heating rate of 5 °C/min.

The bulk densities of the sintered ceramics were measured by Archimedes' method. The crystal structures were analyzed using X-ray powder diffraction (XRPD) with Cu Ka radiation (Rigaku D/MAX2550, Tokyo, Japan). The XRPD data for Rietveld refinement were collected over the range of $2\theta = 10°$–$100°$, with a step size of 0.01° and a count time of 2 s. The Rietveld structure calculations were carried out with the GSAS-EXPGUI program [13]. The Raman spectra were collected at room temperature using a Raman Microscope (Horiba Jobin–Yvon S.A.S., France) with He–Ne laser (633 nm) operated at 30 mw. The microstructure of pellets was investigated using a scanning electron microscope (SEM, Fei Quanta 200, Eindhoven, Holland) coupled with energy dispersive X-ray spectroscopy (EDS). The grain sizes in the samples were obtained from SEM micrographs using the Image Tool software for Windows. (version 3.00; Microsoft, Redmond, WA). The microwave dielectric properties of sintered samples were measured using a network analysis (ZVB20, Rohde and schwarz, Munich, Germany) with the $TE_{01\delta}$ shielded cavity method. The temperature coefficient of resonant frequency (τ_f) was calculated with the following equation:

$$\tau_f = \frac{f_{80} - f_{20}}{f_{20} \times (80 - 20)} \quad (1)$$

where f_{80} and f_{20} are the resonant frequency at 80 and 20 °C, respectively.

3 Results and discussion

Figure 1 depicts the XRPD patterns of $Ca_5Mn_4(VO_4)_6$ ceramics sintered at different temperatures. For the specimens sintered at 825–875 °C, the XRPD diffraction patterns indicated that the cubic structured $Ca_5Mn_4(VO_4)_6$ (JCPDS#06-0494) was identified as a major phase

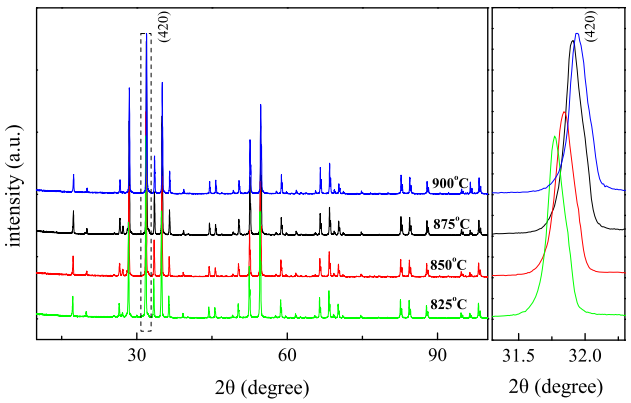

Fig. 1 XRPD patterns of $Ca_5Mn_4(VO_4)_6$ ceramics sintered at different temperatures

combined with a small amount of V-rich secondary phase. Pure phase $Ca_5Mn_4(VO_4)_6$ could be obtained for the sample sintered at 900 °C. Of particular note is that the main peak (420) of $Ca_5Mn_4(VO_4)_6$ shifted toward higher angles with increasing firing temperatures. Herein, Rietveld refinement was employed to illustrate such anomaly. The refinement results of $Ca_5Mn_4(VO_4)_6$ sintered at various temperatures are presented in Fig. 2. The refined lattice parameters and reliable factors are listed in Table 1. It can be clearly seen from Table 1, with the increment of sintering temperature, the lattice parameters of $Ca_5Mn_4(VO_4)_6$ compounds declined slightly, which could be related to the evaporation of vanadium [12, 14].

The room-temperature Raman spectra of $Ca_5Mn_4(VO_4)_6$ ceramics sintered at 875 °C is presented in Fig. 3. The vibration modes in the Raman spectra of the $Ca_5Mn_4(VO_4)_6$ ceramics are classified into two groups, internal and

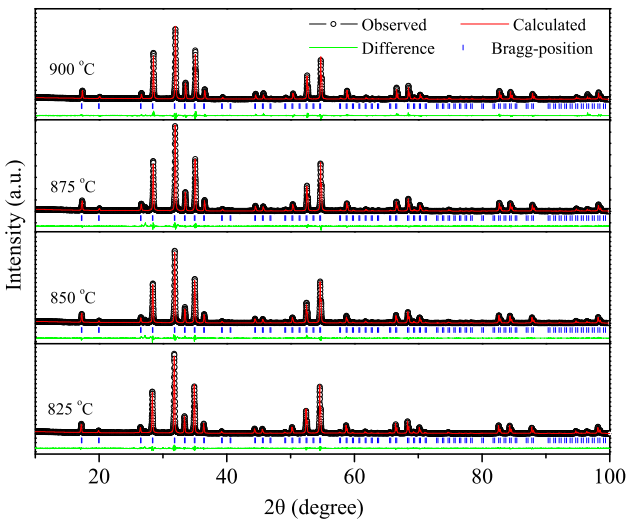

Fig. 2 Rietveld refinement patterns of $Ca_5Mn_4(VO_4)_6$ ceramics sintered at various temperatures

Table 1 Lattice parameters, reliability factors and goodness of fit indicator of $Ca_5M_4(VO_4)_6$ ceramics with different sintering temperatures

ST (°C)	Lattice parameters (Å) a = b = c	R_{wp}	R_p	χ^2
825	12.580415 (29)	12.63	9.58	4.586
850	12.562954 (39)	12.58	8.52	4.703
875	12.544651 (21)	11.46	7.45	4.432
900	12.536175 (31)	9.92	6.80	3.125

Rwp the reliability factor of weighted patterns, *Rp* the reliability factor of patterns, χ^2 goodness of fit indicator = $(Rwp/Rexp)^2$

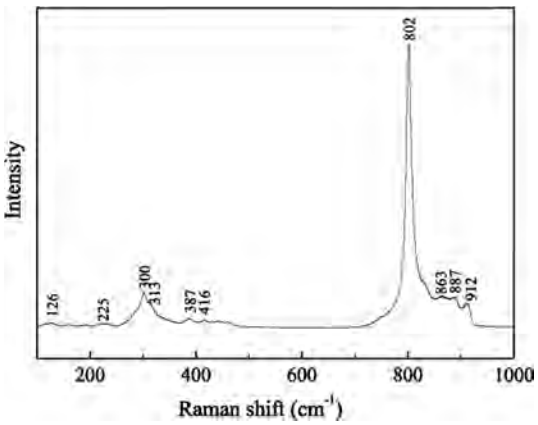

Fig. 3 The room-temperature Raman spectra of $Ca_5Mn_4(VO_4)_6$ ceramics sintered at 875 °C

external. The internal modes are related to the $[VO_4]^{3-}$ molecular group with a stationary mass center, the external modes are associated with the translational motions of the Ca^{2+} and Mn^{2+} cations and rigid molecular units. The Raman band observed in the 912 cm^{-1} can be assigned to the internal symmetric stretching vibration of $(VO_4)^{3-}$ ions, whereas the Raman bands in the 900–750 cm^{-1} region can be identified as the internal anti-symmetric stretching vibration of $(VO_4)^{3-}$ ions [3, 15]. The symmetric bending vibrations of $(VO_4)^{3-}$ anions are observed in the region between 470 and 300 cm^{-1} [16]. The bands observed below 300 cm^{-1} are attributed to the external modes [17].

Typical SEM micrographs of the surfaces of $Ca_5Mn_4(VO_4)_6$ ceramics sintered at various temperatures are illustrated in Fig. 4. As shown in Fig. 4a, a porous structure was clearly found in the sample sintered at 825 °C. With the increment of sintering temperature, the grain size increased continuously along with the decrement in porosity. For the specimen sintered at 875 °C, a dense microstructure with average grain size around 8 um could be achieved. However, abnormal grain growth occurred thereafter, as seen in Fig. 4d. The abnormal grain growth behavior tended to lower the sintering driving force for densification and inhibit extraction of pores from green bodies, which increased the intra granular pores of the grains. As a consequence, the density decreased while the lattice imperfection increased, thus the microwave dielectric properties deteriorated. In addition, all the specimens exhibited two kinds of grains. Combined with the EDS and XRD analysis, the large grains and small grains were identified as $Ca_5Mn_4(VO_4)_6$ and V-rich secondary phase, respectively, as seen in Fig. 4c.

Figure 5 shows the variations in the relative density, ε_r, Q × f, and τ_f of $Ca_5Mn_4(VO_4)_6$ ceramics sintered at different temperatures for 5 h. For all samples, the relative densities first increased and then declined with increasing sintering temperature. The increase of relative density was mainly a result of the less pores and grain growth while the reduction of relative density was due to the abnormal grain growth, as mentioned above. The τ_f values of the samples did not change remarkably with increasing sintering temperature and remained stable at about −70 ppm/°C, because there was no alternate composition at different temperatures [18]. Figure 5b shows the experimental (solid lines) and porosity-corrected values (dot lines) of ε_r calculated using the relation proposed by Hanai et al. [19]. As expected, the variation trend of ε_r followed the same tendency as that of relative density, since higher bulk density means lower porosity ($\varepsilon_r = 1$). The porosity corrected values are slightly higher than the experimentally measured values, as illustrated in Fig. 5b. Generally, Q × f of a composition depends on intrinsic parameters such as structural characteristics (packing fraction and the nature of bonding) and extrinsic parameters such as porosity, secondary phases, grain morphology and size [20–22]. As seen in Fig. 5c, the tendency of Q × f values for all specimens showed a similar trend as that of the relative density, suggesting that densification plays an important role in the extrinsic factors. In addition, Kim et al. [23] reported that the Q × f value increased with the increase of packing fraction due to the decrease of lattice vibrations. In the present investigation, the packing fractions of $Ca_5Mn_4(VO_4)_6$ ceramics have been calculated using the relation given by,

$$\text{Packing fraction } (\%) = \frac{\textit{volume of packed ions}}{\textit{volume of unit cell}} \times Z \qquad (2)$$

where Z is the number of formula units per unit cell of the compound. The calculated results are shown in Fig. 5c, which keep a good consistence with the Q × f values as a function of sintering temperature, except $Ca_5Mn_4(VO_4)_6$ at 900 °C. Therefore, the initial increase in Q × f values of all samples could be ascribed to the consequence of the synergistical effect between high relative density and packing fraction, whereas its degradation at higher

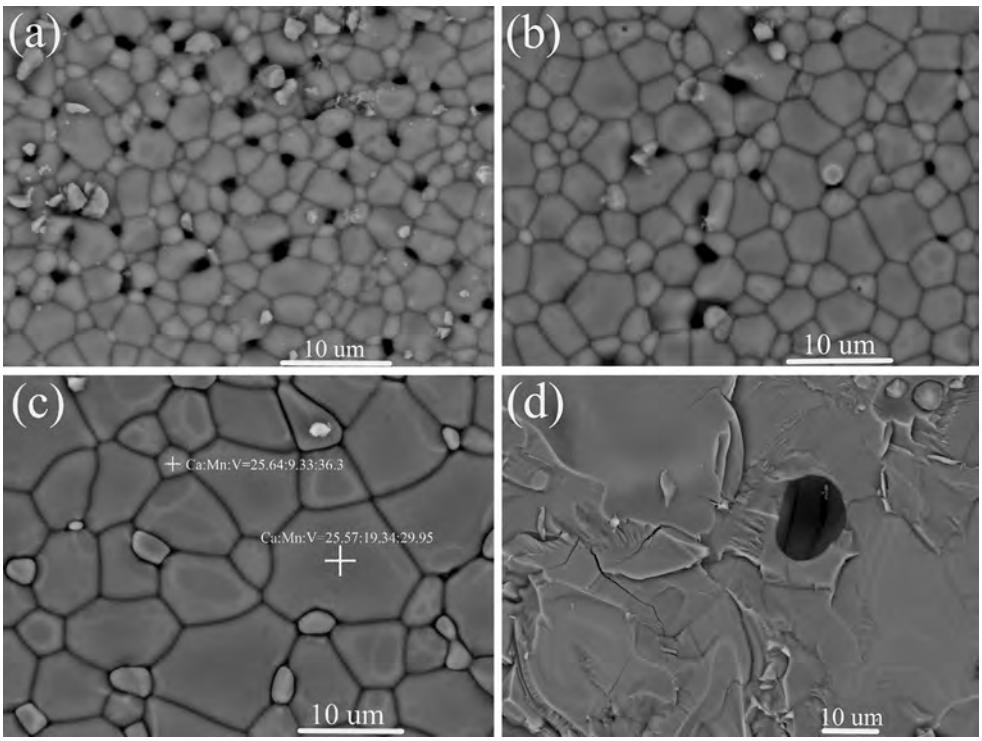

Fig. 4 Typical SEM images of $Ca_5Mn_4(VO_4)_6$ ceramics sintered at: **a** 825 °C, **b** 850 °C, **c** 875 °C, and **d** 900 °C

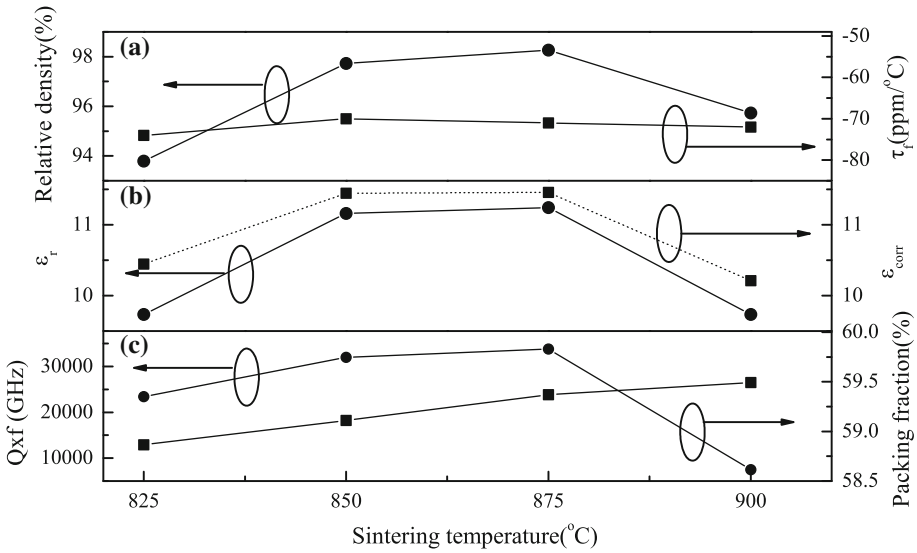

Fig. 5 Variation of relative density and microwave dielectric properties of $Ca_5Mn_4(VO_4)_6$ ceramics as a function of sintering temperature

temperatures might be related to the poor densification as well as the lattice defects caused by abnormal grain growth [24], as discussed before.

It is worth mention that for LTCC applications a $Q \times f \sim 1000$ GHz is often sufficient, as the major contribution to the dielectric losses arises from the metallic circuitry [25]. Therefore, it is necessary to study the chemical compatibility of $Ca_5Mn_4(VO_4)_6$ ceramics with silver, to evaluate their potential as LTCC materials. Figure 6 exhibits the XRPD patterns of $Ca_5Mn_4(VO_4)_6$ calcined powder with 20 wt% Ag addition sintered at 875 °C. As shown in Fig. 6, the main phase $Ca_5Mn_4(VO_4)_6$ disappeared and a new main phase $(AgCa_2)Mn_2(VO_4)_3$ (JCPDS#88-1527) was formed. This indicated that the serious chemical reaction between $Ca_5Mn_4(VO_4)_6$ powders and Ag electrode occurred, which would impede the further application of $Ca_5Mn_4(VO_4)_6$ ceramics for LTCC.

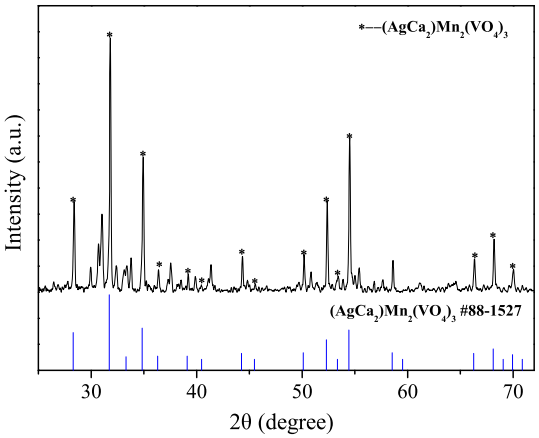

Fig. 6 XRPD pattern of $Ca_5Mn_4(VO_4)_6$–20 wt% Ag sample sintered at 875 °C for 5 h

4 Conclusions

Garnet structure $Ca_5Mn_4(VO_4)_6$ microwave dielectric ceramics with low firing temperature were synthesized by a conventional solid-state method. Phase constitution was confirmed by the XRPD and Raman results. For $Ca_5Mn_4(VO_4)_6$, it is seemed that its ε_r is mainly affected by relative density, while its $Q \times f$ seems to be mainly dominated by intrinsic (packing fraction) and extrinsic (relative density) factors. The typical values of $\varepsilon_r = 11.2$, $Q \times f = 33\ 800$ GHz (at 10.5 GHz), and $\tau_f = -70$ ppm/°C were obtained for $Ca_5Mn_4(VO_4)_6$ ceramic at 875 °C/5 h, wherwas the serious chemical reaction between $Ca_5Mn_4(VO_4)_6$ and Ag substantially affected its commercial viability for LTCC applications.

Acknowledgments This work is supported by the National Natural Science Foundation of China (Grants Nos. 51402235, 51272150, and 51132003). The Natural Science Foundation of Shaanxi Provence, China (Grant No. 2015JQ5143).

References

1. M.R. Joung, J.S. Kim, S. Nahm, J. Am. Ceram. Soc. **92**, 3092 (2009)
2. Y.C. Chen, H.M. You, J. Mater. Sci. Mater. Electron. **27**, 1493 (2016)
3. U.A. Neelakantan, S.E. Kalathil, R. Ratheesh, Eur. J. Inorg. Chem. **2**, 305 (2015)
4. M. Ohashi, H. Ogawa, E. Tanaka, J. Eur. Ceram. Soc. **25**, 2877 (2005)
5. D. Song, C.F. Guo, T. Li, Ceram. Int. **41**, 6518 (2015)
6. L. Fang, H.F. Zhou, H. Zhang, J. Am. Ceram. Soc. **96**, 688 (2013)
7. Y.L. Huang, Y.M. Yu, H.J. Seo, Opt. Express **20**, 4360 (2012)
8. L. Fang, C.X. Su, F. Xiang, H. Zhang, Ceram. Int. **39**, 9779 (2013)
9. E.B. Slobodin, A.A. FotiCv, N.G. Sharova, Zh. Neorg. Khim. **23**, 184 (1978)
10. H.F. Zhou, Y.B. Miao, X.L. Chen, J. Mater. Sci. Mater. Electron. **25**, 2470 (2014)
11. G.G. Yao, P. Liu, H.W. Zhang, J. Am. Ceram. Soc. **96**, 1691 (2013)
12. G.G. Yao, P. Liu, H.W. Zhang, J. Eur. Ceram. Soc. **34**, 2983 (2014)
13. A.C. Larson, R.B. Von Dreele, Los Alamos National Laboratory Report LAUR, **86** (2004)
14. Y. Wang, R.Z. Zuo, J. Eur. Ceram. Soc. **36**, 247 (2016)
15. M. Azdouz, B. Manouna, R. Essehli, L. Biha, J. Alloys Compds. **648**, 368 (2015)
16. A. Grzechnik, P.F. McMillan, J. Solid State Chem. **132**, 156 (1997)
17. S. Benmokhtar, A.E. Jazouli, J. Solid State Chem. **177**, 4175 (2004)
18. E.L. Colla, I.M. Reaney, N. Setter, J. Appl. Phys. **74**, 3414 (1993)
19. T. Hanai, Kolloid Z. **171**, 23 (1960)
20. H. Tamura, Am. Ceram. Soc. Bull. **73**, 92 (1994)
21. P. Zhang, Y.G. Zhao, Mater. Lett. **161**, 620 (2015)
22. M. Valant, D. Suvorov, Mater. Chem. Phys. **79**, 104 (2003)
23. E.S. Kim, B.S. Chun, R. Freer, R.J. Cernik, J. Eur. Ceram. Soc. **30**, 1731 (2010)
24. R.C. Pullar, J. Am. Ceram. Soc. **92**, 563 (2009)
25. G. Schileo, A. Dias, R.L. Moreira, P.A. Smith, A. Feteira, J. Am. Ceram. Soc. **97**, 1096 (2014)